

Spin qubits in graphene quantum dots

Björn Trauzettel, Denis V. Bulaev, Daniel Loss, and Guido Burkard

Department of Physics and Astronomy, University of Basel, Klingelbergstrasse 82, CH-4056 Basel, Switzerland

(Dated: January 2007)

The electron spin is a very promising candidate for a solid-state qubit [1]. Major experimental breakthroughs have been achieved in recent years using quantum dots formed in semiconductor heterostructures based on GaAs technology [2, 3, 4, 5]. In such devices, the major sources of spin decoherence have been identified as the spin-orbit interaction, coupling the spin to lattice vibrations [6, 7, 8], and the hyperfine interaction of the electron spin with the surrounding nuclear spins [9, 10, 11, 12, 13, 14]. Therefore, it is desirable to form qubits in quantum dots based on other materials, where spin-orbit coupling and hyperfine interaction are considerably weaker [15]. It is well known that carbon-based materials such as nanotubes or graphene are excellent candidates. This is so because spin-orbit coupling is weak in carbon due to its relatively low atomic weight, and because natural carbon consists predominantly of the zero-spin isotope ^{12}C , for which the hyperfine interaction is absent. Here we show how to form spin qubits in graphene. A crucial requirement to achieve this goal is to find quantum dot states where the usual valley degeneracy is lifted. We show that this problem can be avoided in quantum dots with so-called armchair boundaries. We furthermore show that spin qubits in graphene can not only be coupled (via Heisenberg exchange) between nearest neighbor quantum dots but also over long distances. This remarkable feature is a direct consequence of the Klein paradox being a distinct property of the quasi-relativistic spectrum of graphene. Therefore, the proposed system is ideal for fault-tolerant quantum computation, and thus for scalability, since it offers a low error rate due to weak decoherence, in combination with a high error threshold due to the possibility of long-range coupling.

Only very recently, the fabrication of a single layer of graphene and the measurement of its electric transport properties have been achieved [16, 17, 18]. Two fundamental problems need to be overcome before graphene can be used to form spin qubits and to operate one or two of them as proposed in Refs. [1, 9]: (i) It is difficult to create a tunable quantum dot in graphene because of the absence of a gap in the spectrum. The phenomenon of Klein tunnelling makes it hard to confine particles [19, 20, 21]. (ii) Due to the valley degeneracy that exists in graphene [22, 23, 24], it is non-trivial to form two-qubit gates using Heisenberg exchange coupling for spins in tunnel-coupled dots. Several attempts have been made to solve the problem (i) such as to use suitable transverse states in graphene ribbons to confine electrons [25], to combine single and bilayer regions of graphene [26], or to achieve confinement by using inhomogeneous magnetic fields [27]. The problem (ii) has not been recognized up to now. Here we propose a setup which solves both problems (i) and (ii) at once. Similar to Ref. [25] we choose to confine electrons

by using suitable transverse states in a ribbon of graphene, cf. Fig. 1. In particular, we assume *semiconducting armchair* boundary conditions to exist on two opposite edges of the sample. It is by now feasible to experimentally identify ribbons of graphene with specific boundaries on the atomic scale. These are preferably of zigzag or of armchair type. For an experimental realization of our proposal, one would have to look for ribbons with semiconducting armchair boundaries. It is known that in such a device the valley degeneracy is lifted [28, 29], which is the essential prerequisite for the appearance of Heisenberg exchange coupling for spins in tunnel-coupled quantum dots (see below), and thus for the use of graphene dots for spin qubits. We show below that spin qubits in graphene can not only be coupled between nearest neighbor quantum dots but also over long distances. This long-distance coupling mechanism makes use of conduction band to valence band tunnelling processes and is, therefore, directly based on the Klein paradox in graphene [20, 21].

We now discuss bound-state solutions in our setup, which are required for a localized qubit. We first concentrate on a single quantum dot which is assumed to be rectangular with width W and length L , see Fig. 1. The basic idea of forming the dot is to take a ribbon of graphene with semiconducting armchair boundary conditions in x -direction and to electrically confine particles in y -direction. The low energy properties of electrons (with energy ε with respect to the Dirac point) in such a setup are described by the 4×4 Dirac equation

$$-i\hbar v \begin{pmatrix} \sigma_x \partial_x + \sigma_y \partial_y & 0 \\ 0 & -\sigma_x \partial_x + \sigma_y \partial_y \end{pmatrix} \Psi + eV(y)\Psi = \varepsilon \Psi, \quad (1)$$

where the electric gate potential is assumed to vary stepwise, $V(y) = V_{\text{gate}}$ in the dot region (where $0 \leq y \leq L$), and $V(y) = V_{\text{barrier}}$ in the barrier region (where $y < 0$ or $y > L$). In Eq. (1), σ_x and σ_y are Pauli matrices, \hbar is Planck's constant divided by 2π , v the Fermi velocity, and e the charge of an electron. The four component spinor envelope wave function $\Psi = (\Psi_A^{(K)}, \Psi_B^{(K)}, -\Psi_A^{(K')}, -\Psi_B^{(K')})$ varies on scales large compared to the lattice spacing. At this point, we are only interested in the orbital structure of the wave function. The spin degree of freedom is neglected until the final part, where we discuss the Heisenberg exchange coupling for spins in tunnel-coupled quantum dots. In the wave function Ψ , A and B refer to the two sublattices in the two-dimensional honeycomb lattice of carbon atoms, whereas K and K' refer to the vectors \mathbf{K} and \mathbf{K}' in reciprocal space corresponding to the two valleys in the bandstructure of graphene. The appropriate semiconducting armchair boundary conditions for such a wave function have been formulated in Ref. [28] and can be written as ($\alpha = A, B$)

$$\Psi_\alpha^{(K)}|_{x=0} = \Psi_\alpha^{(K')}|_{x=0}, \quad \Psi_\alpha^{(K)}|_{x=W} = e^{\pm 2\pi/3} \Psi_\alpha^{(K')}|_{x=W}, \quad (2)$$

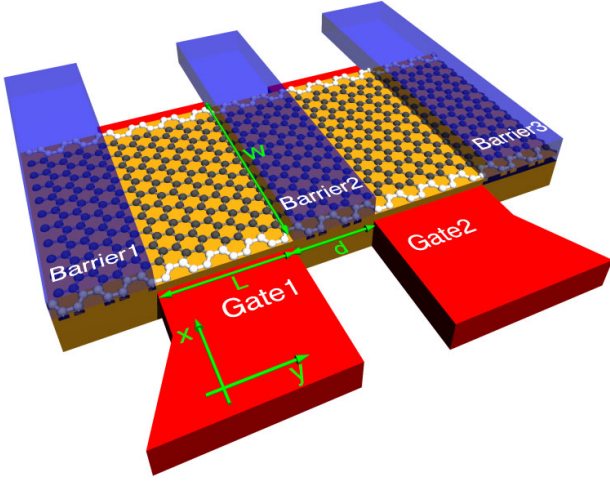


FIG. 1: **Schematic of a graphene double quantum dot.** Each dot is assumed to have length L and width W . The structure is based on a ribbon of graphene (grey) with semiconducting armchair edges (white). Confinement is achieved by tuning the voltages applied to the “barrier” gates (blue) to appropriate values such that bound states exist. Additional gates (red) allow to shift the energy levels of the dots. Virtual hopping of electrons through barrier 2 (thickness d) gives rise to a tunable exchange coupling J between two electron spins localized in the left and the right dot. The exchange coupling is then used to generate universal two-qubit gates.

corresponding to a width W of the ribbon shown in Fig. 1, where W is not an integer multiple of three unit cells. The \pm signs in Eq. (2) (as well as in Eq. (3) below) correspond to the two possible choices of a number of unit cells that is not an integer multiple of three. The full set of plane wave solutions of Eq. (1) is readily determined [29]. It is well known that the boundary condition (2) yields the following quantization conditions for the wave vector $k_x \equiv q_n$ in x -direction [28, 29]

$$q_n = (n \pm 1/3)\pi/W, \quad n \in \mathbb{Z}. \quad (3)$$

An explicit form of the corresponding wave functions is presented in App. A and App. B. The level spacing of the modes (3) can be estimated as $\Delta\varepsilon \approx \hbar v\pi/3W$, which gives $\Delta\varepsilon \approx 30$ meV, where we used that $v \approx 10^6$ m/s and assumed a quantum dot width of about $W \approx 30$ nm. Note that Eq. (3) also determines the energy gap for excitations as $E_{\text{gap}} = 2\hbar vq_0$. Therefore, this gap is of the order of 60 meV, which is unusually small for semiconductors. This is a unique feature of graphene that will allow for long-distance coupling of spin qubits as will be discussed below.

We now present in more detail the ground-state solutions, i.e. $n = 0$ in Eq. (3). The corresponding ground-state energy ε can be expressed relative to the potential barrier $V = V_{\text{barrier}}$ in the regions $y < 0$ and $y > L$ as $\varepsilon = eV_{\text{barrier}} \pm \hbar v(q_0^2 + k^2)^{1/2}$. Here, the \pm sign refers to a conduction band (+) and a valence band (−) solution to Eq. (1). For bound states to exist and to decay at $y \rightarrow \pm\infty$, we require that $\hbar vq_0 > |\varepsilon - eV_{\text{barrier}}|$, which implies that the wave vector $k_y \equiv k$ in y -direction, given by

$$k = i\sqrt{q_0^2 - ((\varepsilon - eV_{\text{barrier}})/\hbar v)^2}, \quad (4)$$

is purely imaginary. In the dot region ($0 \leq y \leq L$), the wave vector k in y -direction is replaced by \tilde{k} , satisfying $\varepsilon = eV_{\text{gate}} \pm \hbar v(q_0^2 + \tilde{k}^2)^{1/2}$. Again the \pm sign refers to conduction and valence band solutions. In the following, we focus on conduction band solutions to the problem.

Since the Dirac equation (1) implies the continuity of the wave function, the matching condition at $y = 0$ and $y = L$ allows us to derive the transcendental equation for ε

$$e^{2i\tilde{k}L}(z_{0,k} - z_{0,\tilde{k}})^2 - (1 - z_{0,k}z_{0,\tilde{k}})^2 = 0 \quad (5)$$

with $z_{0,k} \equiv (q_0 + ik)/(q_0^2 + k^2)^{1/2}$. Eq. (5) determines the allowed energies ε for bound states. In order to analyze the solutions to Eq. (5), we distinguish two cases, one where \tilde{k} is real, and the other, where \tilde{k} is purely imaginary. The two cases are distinguished by the condition $|\varepsilon - eV_{\text{gate}}| \geq \hbar vq_0$ and $|\varepsilon - eV_{\text{gate}}| < \hbar vq_0$, respectively. Furthermore, we assume that $V_{\text{gate}} \neq V_{\text{barrier}}$, i.e., $z_{0,k} \neq z_{0,\tilde{k}}$. If we relax this assumption, we can show that for the case $z_{0,k} = z_{0,\tilde{k}}$ only a single solution to Eq. (5) exists, namely $z_{0,\tilde{k}} = 1$, which implies that $\tilde{k} = 0$. The corresponding wave function to this solution vanishes identically (see App. A for further details). In the case where \tilde{k} is purely imaginary, there is no bound-state solution. This is due to the fact that such a solution would have to exist directly in the bandgap. We now analyze solutions for real \tilde{k} . In the corresponding energy window

$$|\varepsilon - eV_{\text{gate}}| \geq \hbar vq_0 > |\varepsilon - eV_{\text{barrier}}|, \quad (6)$$

we can simplify Eq. (5) considerably, obtaining

$$\tan(\tilde{k}L) = \frac{\hbar v\tilde{k} \sqrt{(\hbar vq_0)^2 - (\varepsilon - eV_{\text{barrier}})^2}}{(\varepsilon - eV_{\text{barrier}})(\varepsilon - eV_{\text{gate}}) - (\hbar vq_0)^2}. \quad (7)$$

We show a set of solutions to Eq. (7) for a relatively short dot ($q_0L = 2$) as well as a longer dot ($q_0L = 5$) in Fig. 2. The number of bound states N (for $n = 0$) is maximal if $\Delta V = V_{\text{barrier}} - V_{\text{gate}}$ is exactly as large as the size of the gap $E_{\text{gap}} = 2\hbar vq_0$, then $N_{\text{max}} = \lceil \sqrt{8}q_0L/\pi \rceil$, where $\lceil x \rceil$ is the integer just larger than x . The level spacing associated with the allowed solutions of Eq. (7) increases as L decreases and has a rather complicated parameter dependence. It can, however, be estimated to be of the order of $\Delta\varepsilon \approx \hbar v\pi/\max\{W, L\}$, which is in the energy range of a few tens of meV as mentioned below Eq. (3). In Fig. 3, we show the energy bands of a single dot and two neighboring barrier regions as well as a double dot setup with three barrier regions. The double dot case illustrates how we make use of the Klein paradox to couple two dots.

A particular example of a wave function is shown in Fig. 4. It is a ground-state solution under the parameter choice $e(V_{\text{barrier}} - V_{\text{gate}}) = 0.6\hbar vq_0$, and $q_0L = 2$ (indicated by the arrow in Fig. 2). The weight of the wave function on the A and B lattice sites is different, however, the integrated weight is the same as required by the normalization condition [28]. Ground-state solutions (i.e. the lowest lying (red) lines in Fig. 2) have no nodes in the dot region – similar to the corresponding problem of confined electrons that obey the non-relativistic Schrödinger equation. Excited-state solutions in

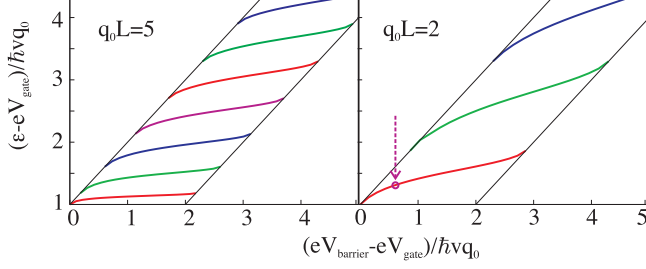


FIG. 2: **Bound state solutions for two different dot sizes.** Bound-state solutions of a relatively long ($q_0 L = 5$, left panel) and a shorter ($q_0 L = 2$, right panel) quantum dot are shown. The diagonal straight lines mark the area in which bound-state solutions can occur. The arrow marks the solution for which the wave function is plotted in Fig. 4.

parameter regions in which they exist, do have nodes in the dot region, which is shown in Fig. 8 of App. C.

We now turn to the case of two coupled graphene quantum dots, separated by a potential barrier, as sketched in Fig. 1, each dot filled with a single electron. It is interesting to ask whether the spins \mathbf{S}_i of these two electrons ($i = 1, 2$) are coupled through an exchange coupling, $H_{\text{exch}} = \mathbf{J} \mathbf{S}_1 \cdot \mathbf{S}_2$, in the same way as for regular semiconductor quantum dots [9], because this coupling is, in combination with single-spin rotations, sufficient to generate all quantum gates required for universal quantum computation [1]. The exchange coupling is based on the Pauli exclusion principle which allows for electron hopping between the dots in the spin singlet state (with opposite spins) of two electrons, but not in a spin triplet (with parallel spins), thus leading to a singlet-triplet splitting (exchange energy) J . However, a singlet-triplet splitting $J \neq 0$ only occurs if the triplet state with two electrons on the same dot in the ground state is forbidden, i.e., in the case of a single *non-degenerate* orbital level. This is a non-trivial requirement in a graphene structure, as in bulk graphene, there is a two-fold orbital (“valley”) degeneracy of states around the points \mathbf{K} and \mathbf{K}' in the first Brillouin zone. This valley degeneracy is lifted in our case of a ribbon with *semiconducting armchair edges*, and the ground-state solutions determined by Eq. (7) are in fact non-degenerate. The magnitude of the exchange coupling within a Hund-Mulliken model is [9] $J = (-U_H + (U_H^2 + 16t_H^2)^{1/2})/2 + V$, where t is the tunnelling (hopping) matrix element between the left and right dot, U is the on-site Coulomb energy, and V is the direct exchange from the long-range (inter-dot) Coulomb interaction. The symbols t_H and U_H indicate that these quantities are renormalized from the bare values t and U by the inter-dot Coulomb interaction. For $t \ll U$ and neglecting the long-ranged Coulomb part, this simplifies to the Hubbard model result $J = 4t^2/U$ where t is the tunnelling (hopping) matrix element between the left and right dot and U is the on-site Coulomb energy. In the regime of weak tunnelling, we can estimate $t \approx \varepsilon \int \Psi_L^\dagger(x, y) \Psi_R(x, y) dx dy$, where $\Psi_{L,R}(x, y) = \Psi(x, y \pm (d + L)/2)$ are the ground-state spinor

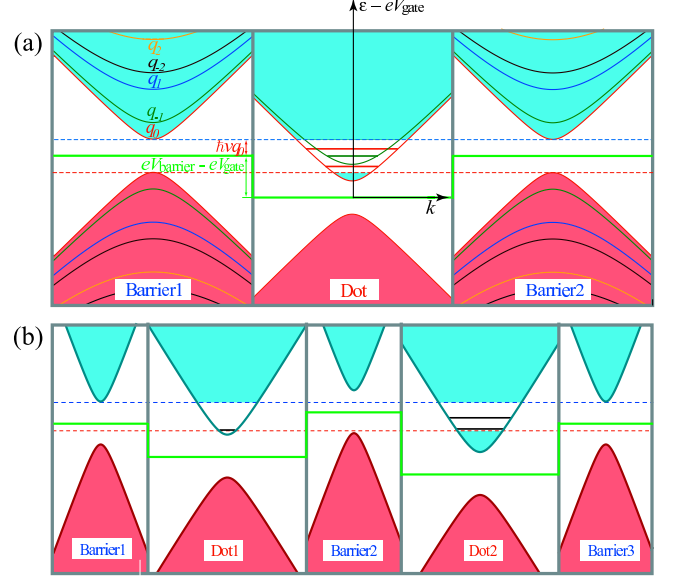


FIG. 3: **Energy bands for single and double dot case.** (a) Energy bands for two barrier regions and a single dot. The red area marks a continuum of states in the valence bands and the blue area marks a continuum of states in the conduction bands. In the barrier regions, we indicate the energy bands of the quantized modes due to transverse confinement. All modes are non-degenerate solutions in valley space. They come pairwise in a sense that always two of them are separated by a distance $\hbar v q_0$ in energy space. In the figure, this is illustrated for the energy levels corresponding to wave vectors q_0 and q_{-1} as well as q_1 and q_{-2} . In the dot region, the electric confinement in longitudinal direction yields an additional level structure, i.e. the one shown in Fig. 2. For clarity, we only show the dot levels that are located in the gap of the barrier regions and are, therefore, bound states. In the figure, we choose to present a situation with three bound states in total: Two of them are of the $n = 0$ series (straight red lines in the center region) and a single one is of the $n = -1$ series (straight green line in the center region). (b) Energy bands for a double dot setup. A single bound state (straight black line) is shown in the conduction band of the left dot and two bound states are shown in the conduction band of the right dot. They are coupled via the continuum in the valence band of the central barrier which is enabled by the Klein paradox.

wave functions of the left and right dots and ε is the single-particle ground state energy. Note that the overlap integral vanishes if the states on the left and right dot belong to different transverse quantum numbers $q_{n_L} \neq q_{n_R}$. For the ground state mode, we have $n_L = n_R = 0$, and the hopping matrix element can be estimated for $d \gtrsim L$ as

$$t \approx 4\varepsilon\alpha_0\delta_0^* W d z_{0,k} \exp(-d|k|), \quad (8)$$

where α_0 and δ_0 are wave function amplitudes (with dimension 1/length) that are specified in App. C. As expected, the exchange coupling decreases exponentially with the barrier thickness, the exponent given by the “forbidden” momentum k in the barrier, defined in Eq. (4). The amplitude t can be maximized by tuning to a bound-state solution, where

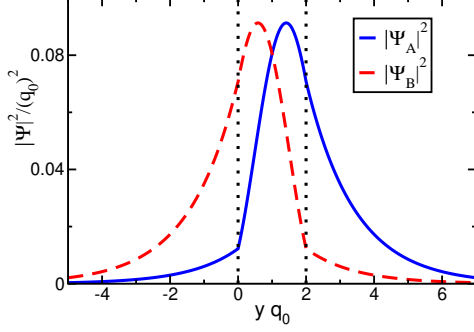


FIG. 4: **Ground-state wave function.** Normalized squared wave functions $|\Psi_A|^2 = |\Psi_A^{(K)}|^2 = |\Psi_A^{(K')}|^2$ and $|\Psi_B|^2 = |\Psi_B^{(K)}|^2 = |\Psi_B^{(K')}|^2$ for the bound state solution for the parameter choice $e(V_{\text{barrier}} - V_{\text{gate}}) = 0.6\hbar v q_0$, and $q_0 L = (\pi/3)L/W = 2$ (indicated by the arrow in Fig. 2). The corresponding energy is given by $\varepsilon \approx 1.31 \cdot \hbar v q_0$. The dotted lines indicate the dot region $0 \leq y \leq L$.

$|\varepsilon - eV_{\text{barrier}}|$ approaches $\hbar v q_0$ (from below). Then, $d|k| < 1$. Such a fine-tuning can be easily achieved in graphene quantum dots, where the small band gap allows to sweep through it and, therefore, to use conduction and valence band states (of the barrier region) to couple quantum dots. In Fig. 3(b), we sketch the energy bands for the double dot case which shows how confined states in the two dots can be coupled via cotunnelling processes through the continuum of states in the valence band of the central barrier region. Remarkably, this opens up the possibility for long distance coupling of electron spins because, in the limit $|\varepsilon - eV_{\text{barrier}}| \rightarrow \hbar v q_0$, the coupling t depends only weakly on the distance d between the quantum dots. However, already for bound state solutions with $|k|d > 1$, a coupling over a length exceeding several times the dot size is possible. For the situation where we couple two ground states in the quantum dots, we find, for instance, a solution, where $|k|d = 4$, $d = 10L$, and the coupling can still be as large as $t \approx 0.03\varepsilon$ for highly localized qubits. This example is shown in Fig. 5. If we couple a ground state in the one dot with an excited state in the other dot, the hopping matrix element t can be even larger. The corresponding wave functions for that case are illustrated in Fig. 9. The values of t , U , and J can be estimated as follows. The tunnelling matrix element t is a fraction of $\varepsilon \approx 30$ meV (for a width of $W \approx 30$ nm), we obtain that $t \approx 0.5 \dots 2.5$ meV. The value for U depends on screening which we can assume to be relatively weak in graphene [24], thus, we estimate, e.g., $U \approx 10$ meV, and obtain $J \approx 0.1 \dots 1.5$ meV.

For the situation with more than two dots in a line, it turns out that we can couple any two of them with the others being decoupled by detuning. We mention here that our model is based on a single particle picture. Such a model effectively captures effects of Coulomb interactions as far as they can be described within the constant interaction model for quantum dots [30]. The Coulomb interaction then only shifts the energy levels in each dot by a constant. In Fig. 6, we illustrate the situation of three dots in a line where the left and the right dot are

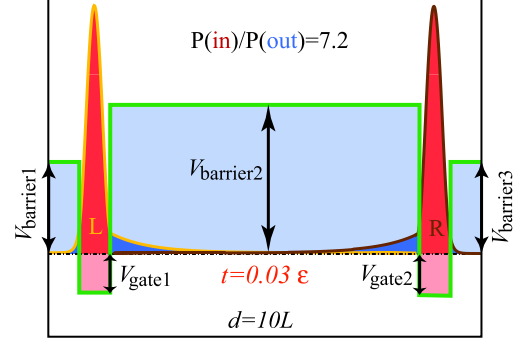


FIG. 5: **Long-distance coupling of two qubit ground states.** The normalized squared wave functions $|\Psi|^2 = |\Psi_A^{(K)}|^2 + |\Psi_A^{(K')}|^2 + |\Psi_B^{(K)}|^2 + |\Psi_B^{(K')}|^2$ of two qubits separated by a distance $d = 10L$, where L is the length of each quantum dot, are plotted next to each other. A ground state (of the series with the transverse quantum number $n = 0$) in the left dot is coupled to a ground state (of the same series with $n = 0$) in the right dot. The coupling is as large as $t = 0.03\varepsilon$, where ε is the ground-state energy. Furthermore, the qubits are highly localized, which can be seen from the ratio $P(\text{in})/P(\text{out})$. Here, $P(\text{in})$ is the probability of the electron to be inside the corresponding dot and $P(\text{out})$ is probability to be outside the dot in the barrier regions. The parameters chosen for the potential (in units of $\hbar v q_0/e$) are $V_{\text{barrier}1} = V_{\text{barrier}3} = 1$, $V_{\text{barrier}2} = 1.65$, $V_{\text{gate}1} = V_{\text{gate}2} = -0.5$.

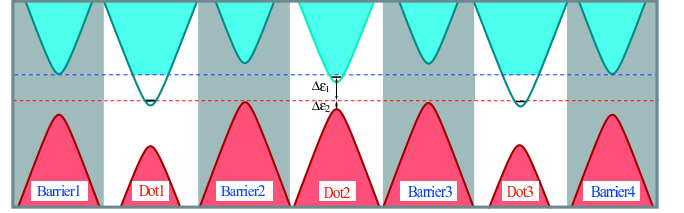


FIG. 6: **Triple quantum dot setup.** The energy bands of a triple quantum dot setup are shown in which dot 1 and dot 3 are strongly coupled via cotunnelling processes through the valence bands of barrier 2, barrier 3, and dot 2. The center dot 2 is decoupled by detuning. The energy levels are chosen such that $\Delta\varepsilon_2 \ll \Delta\varepsilon_1$. The triple dot example illustrates that in a line of quantum dots, it is possible to strongly couple any two of them and decouple the others by detuning. This is a unique feature of graphene and cannot be achieved in semiconductors such as GaAs that have a much larger gap.

strongly coupled and the center dot is decoupled by detuning. The tunnel coupling of dot 1 and dot 3 is then achieved via Klein tunneling through the valence band of the two central barriers and the valence band of the center dot. It is important for the long-distance coupling that the exchange coupling of qubit 1 and qubit 3 is primarily achieved via the valence band and not via the qubit level of the center dot – leaving the qubit state of dot 2 unchanged. Using the standard transition matrix approach, we can compare the transition rate of coupling dot 1 and dot 3 via the continuum of states in the valence band of

the center dot (which we call Γ_{VB}) with the transition rate via the detuned qubit level of the center dot (which we call Γ_{QB}). We obtain for the ratio (see App. D for the derivation)

$$\Gamma_{VB}/\Gamma_{QB} \approx (L/W) \ln(4\Delta/E_{\text{gap}}), \quad (9)$$

where $\Delta \approx 6\text{ eV}$ is the band width of graphene. Therefore, by increasing the aspect ratio L/W , it is possible to increase the rate Γ_{VB} with respect to Γ_{QB} . For $L/W = 2$ and $E_{\text{gap}} = 60\text{ meV}$, we find that $\Gamma_{VB}/\Gamma_{QB} \approx 12$, meaning that the qubit level in dot 2 is barely used to couple dot 1 and dot 3. This is a unique feature of graphene quantum dots due to the small and highly symmetric band gap, which is not known to exist for other semiconducting materials. The availability of non-local interactions is important in the context of quantum error correction, as it raises the error threshold for fault-tolerant quantum computation [31]. In conclusion, we have proposed a setup to form spin qubits in quantum dots based on graphene nanoribbons with semiconducting armchair boundaries. For such a system, we have calculated bound states of a tunable dot and outlined how two-qubit gates can be realized. We expect very long coherence times for such spin qubits since spin-orbit coupling and hyperfine interaction are known to be weak in carbon, see App. E. Furthermore, we have found that the high flexibility in tuning graphene quantum dots in combination with conduction band to valence band tunnelling based on the Klein paradox allows for long distance coupling of electron spins. Therefore, we propose a system which can serve as the fundamental building block for scalable and fault-tolerant quantum computing.

APPENDIX A: GENERAL MODEL

We now present in detail how to derive solutions for bound states in a graphene quantum dot. The dot is assumed to be rectangular with width W and length L as illustrated in Fig. 1. The basic idea of forming the dot is to take a strip of graphene with *semiconducting armchair* boundary conditions in x -direction and to electrically confine particles in y -direction. Transport properties of a similar system have been discussed in Ref. [25].

The low energy properties of electrons with energy ε in such a setup are described by the 4x4 Dirac equation

$$-i\hbar v \begin{pmatrix} \sigma_x \partial_x + \sigma_y \partial_y & 0 \\ 0 & -\sigma_x \partial_x + \sigma_y \partial_y \end{pmatrix} \Psi + eV(y)\Psi = \varepsilon\Psi, \quad (A1)$$

with the electric gate potential

$$V(y) = \begin{cases} V_{\text{gate}}, & (0 \leq y \leq L), \\ V_{\text{barrier}}, & \text{otherwise.} \end{cases} \quad (A2)$$

In Eq. (A1), σ_x and σ_y are Pauli matrices, \hbar is Planck's constant divided by 2π , e is the electron charge, and v is the Fermi velocity. The four component envelope wave function $\Psi = (\Psi_A^{(K)}, \Psi_B^{(K)}, -\Psi_A^{(K')}, -\Psi_B^{(K')})$ varies on scales large compared to the lattice spacing. Here, A and B refer to the two sublattices in the two-dimensional honeycomb lattice of carbon atoms, whereas K and K' refer to the vectors in reciprocal

space corresponding to the two valleys in the bandstructure of graphene.

Plane wave solutions to Eq. (1) take the form [29]

$$\Psi_{n,k}^{(+)}(x, y) = \chi_{n,k}^{(+)}(x) e^{iky}, \quad \Psi_{n,k}^{(-)}(x, y) = \chi_{n,k}^{(-)}(x) e^{-iky} \quad (A3)$$

with

$$\begin{aligned} \chi_{n,k}^{(+)}(x) = & a_{n,+} \begin{pmatrix} 1 \\ z_{n,k} \\ 0 \\ 0 \end{pmatrix} e^{iq_n x} + a'_{n,+} \begin{pmatrix} 0 \\ 0 \\ -z_{n,k} \\ 1 \end{pmatrix} e^{iq_n x} \\ & + b_{n,+} \begin{pmatrix} -z_{n,k} \\ 1 \\ 0 \\ 0 \end{pmatrix} e^{-iq_n x} + b'_{n,+} \begin{pmatrix} 0 \\ 0 \\ 1 \\ z_{n,k} \end{pmatrix} e^{-iq_n x} \end{aligned} \quad (A4)$$

and

$$\begin{aligned} \chi_{n,k}^{(-)}(x) = & a_{n,-} \begin{pmatrix} z_{n,k} \\ 1 \\ 0 \\ 0 \end{pmatrix} e^{iq_n x} + a'_{n,-} \begin{pmatrix} 0 \\ 0 \\ 1 \\ -z_{n,k} \end{pmatrix} e^{iq_n x} \\ & + b_{n,-} \begin{pmatrix} 1 \\ -z_{n,k} \\ 0 \\ 0 \end{pmatrix} e^{-iq_n x} + b'_{n,-} \begin{pmatrix} 0 \\ 0 \\ z_{n,k} \\ 1 \end{pmatrix} e^{-iq_n x}. \end{aligned} \quad (A5)$$

The complex number $z_{n,k}$ is given by

$$z_{n,k} = \pm \frac{q_n + ik}{\sqrt{k^2 + q_n^2}}. \quad (A6)$$

The energy of the state in the barrier regions ($y < 0$ and $y > L$, where $V = V_{\text{barrier}}$) is given by

$$\varepsilon = eV_{\text{barrier}} \pm \hbar v \sqrt{q_n^2 + k^2}. \quad (A7)$$

In the dot ($0 \leq y \leq L$, where $V = V_{\text{gate}}$) the wave vector k is replaced by \tilde{k} , satisfying

$$\varepsilon = eV_{\text{gate}} \pm \hbar v \sqrt{q_n^2 + \tilde{k}^2}. \quad (A8)$$

The \pm sign in Eqs. (A6) – (A8) refers to conduction and valence bands. In the following, we concentrate on conduction band solutions of the problem (keeping in mind that there is always a particle-hole conjugated partner solution).

The transverse wave vector q_n as well as the coefficients $a_{n,\pm}, a'_{n,\pm}, b_{n,\pm}, b'_{n,\pm}$ of the n -th mode are determined (up to a normalization constant) by the boundary conditions at $x = 0$ and $x = W$. We consider a class of boundary conditions for which the resulting parameters are independent of the longitudinal wave vectors k and \tilde{k} . We are particularly interested in semiconducting armchair boundary conditions defined by [28]

$$\Psi|_{x=0} = \begin{pmatrix} 0 & \mathbb{1} \\ \mathbb{1} & 0 \end{pmatrix} \Psi|_{x=0}, \quad (A9)$$

$$\Psi|_{x=W} = \begin{pmatrix} 0 & e^{-i2\pi\mu/3} \mathbb{1} \\ e^{i2\pi\mu/3} \mathbb{1} & 0 \end{pmatrix} \Psi|_{x=W}, \quad (A10)$$

where $\mu = \pm 1$ is defined by the width of the graphene strip $W = a_0(3M + \mu)$, with M a positive integer ($a_0 = 0.246$ nm is the graphene lattice constant), and $\mathbb{1}$ is the 2×2 unit matrix. A strip whose width is an integer multiple of three unit cells ($\mu = 0$) is metallic and not suitable for spin qubit applications. The states of a semiconductor strip are non-degenerate (in valley space):

$$q_n = \frac{\pi}{W}(n + \mu/3), \quad n \in \mathbb{Z} \quad (\text{A11})$$

with $a_{n,\pm} = b'_{n,\pm} = 0$, $a'_{n,\pm} = b_{n,\pm}$ (for $\mu = -1$) or $a'_{n,\pm} = b_{n,\pm} = 0$, $a_{n,\pm} = b'_{n,\pm}$ (for $\mu = 1$). Note that q_n determines the size of the gap for each mode n that is due to the boundary conditions. The size of the gap of mode n is given by $2\hbar v q_n$. For concreteness, we consider the case of $\mu = 1$ only. It can be shown that for the case of $\mu = -1$, the bound states and normalized squared wave functions have exactly the same dependence on the parameters of a quantum dot, V_{barrier} , V_{gate} , W , and L .

Our ansatz for a bound state solution at energy ε to Eq. (1) then reads

$$\Psi = \begin{cases} \alpha'_n \chi_{n,k}^{(-)}(x) e^{-iky}, & \text{if } y < 0, \\ \beta'_n \chi_{n,k}^{(+)}(x) e^{iky} + \gamma'_n \chi_{n,\tilde{k}}^{(-)}(x) e^{-i\tilde{k}y}, & \text{if } 0 \leq y \leq L, \\ \delta'_n \chi_{n,k}^{(+)}(x) e^{ik(y-L)}, & \text{if } y > L. \end{cases} \quad (\text{A12})$$

For bound states, the wave function should decay for $y \rightarrow \pm\infty$, so we require that

$$k = i \sqrt{q_n^2 - (\varepsilon - eV_{\text{barrier}})^2 / (\hbar v)^2}, \quad (\text{A13})$$

where $\hbar v q_n > |\varepsilon - eV_{\text{barrier}}|$ always has to hold.

To find bound state solutions, we have to analyze the following set of equations (coming from wave function matching at $y = 0$ and $y = L$)

$$\begin{aligned} \alpha_n \begin{pmatrix} z_{n,k} \\ 1 \end{pmatrix} &= \beta_n \begin{pmatrix} 1 \\ z_{n,\tilde{k}} \end{pmatrix} + \gamma_n \begin{pmatrix} z_{n,\tilde{k}} \\ 1 \end{pmatrix}, \\ \delta_n \begin{pmatrix} 1 \\ z_{n,k} \end{pmatrix} &= \beta_n \begin{pmatrix} 1 \\ z_{n,\tilde{k}} \end{pmatrix} e^S + \gamma_n \begin{pmatrix} z_{n,\tilde{k}} \\ 1 \end{pmatrix} e^{-S}, \end{aligned} \quad (\text{A14})$$

where $\alpha_n = \alpha'_n a_{n,-}$, $\beta_n = \beta'_n a_{n,+}$, $\gamma_n = \gamma'_n a_{n,-}$, $\delta_n = \delta'_n a_{n,+}$, and $S \equiv i\tilde{k}L$. We can write Eq. (A14) as

$$\begin{pmatrix} z_{n,k} & -1 & -z_{n,\tilde{k}} & 0 \\ 1 & -z_{n,\tilde{k}} & -1 & 0 \\ 0 & -e^S & -z_{n,\tilde{k}} e^{-S} & 1 \\ 0 & -z_{n,\tilde{k}} e^S & -e^{-S} & z_{n,k} \end{pmatrix} \begin{pmatrix} \alpha_n \\ \beta_n \\ \gamma_n \\ \delta_n \end{pmatrix} = 0. \quad (\text{A15})$$

The allowed energy values ε are readily determined by finding the roots of the determinant of the matrix on the lhs of the latter equation

$$e^{2S} (z_{n,k} - z_{n,\tilde{k}})^2 - (1 - z_{n,k} z_{n,\tilde{k}})^2 = 0. \quad (\text{A16})$$

A rather obvious solution is $z_{n,\tilde{k}} = 1$ (which implies that $S = 0$) corresponding to

$$\varepsilon = \pm \hbar v q_n + eV_{\text{gate}}. \quad (\text{A17})$$

However, the corresponding wave functions to the allowed energy solutions (A17) vanish identically. So, in order to proceed, we have to find other (less trivial) solutions to the transcendental equation (A16). Since the case $z_{n,k} = z_{n,\tilde{k}}$ only has the trivial solution (A17), we can assume that $z_{n,k} \neq z_{n,\tilde{k}}$, which means that $V_{\text{barrier}} \neq V_{\text{gate}}$. Then, we find that

$$e^S = \pm \frac{1 - z_{n,k} z_{n,\tilde{k}}}{z_{n,k} - z_{n,\tilde{k}}}. \quad (\text{A18})$$

To analyze the solutions of Eq. (A18), we distinguish two cases, one where

$$S = i\tilde{k}L \quad (\text{A19})$$

is purely imaginary (i.e., \tilde{k} is real), and another, where S is real. The two cases are distinguished by the criterion $|\varepsilon - eV_{\text{gate}}| \geq \hbar v q_n$ and $|\varepsilon - eV_{\text{gate}}| < \hbar v q_n$, respectively. In the former case, since the lhs of Eq. (A18) has modulus unity, also the rhs must be unimodular, which is satisfied if in addition $|\varepsilon - eV_{\text{barrier}}| \leq \hbar v q_n$. This case, where the equation for the argument of Eq. (A18) remains to be solved, is discussed in Sec. B. The latter case where S is real has no solutions.

Indeed, let us rewrite Eq. (A18) as follows:

$$e^{2S} - 1 = \frac{-2\tilde{k}k}{q_n^2 - (\varepsilon - eV_{\text{barrier}})(\varepsilon - eV_{\text{gate}})/(\hbar v)^2 + \tilde{k}k}. \quad (\text{A20})$$

Taking into account that $q_n^2 > (\varepsilon - eV_{\text{barrier}})(\varepsilon - eV_{\text{gate}})/(\hbar v)^2$ and $\tilde{k}k \in \mathbb{R}$, we find that the left and right sides of this equation have different signs, therefore, Eq. (A18) has no roots for any purely imaginary \tilde{k} .

APPENDIX B: BOUND STATE SOLUTIONS

We now restrict ourselves to the energy window

$$|\varepsilon - eV_{\text{gate}}| \geq \hbar v q_n \geq |\varepsilon - eV_{\text{barrier}}|. \quad (\text{B1})$$

Then \tilde{k} is real, therefore $|e^S| = 1$ and $|z_{n,\tilde{k}}| = 1$. Furthermore, $z_{n,k}$ is real. We define $z_{n,\tilde{k}} \equiv e^{i\theta_n}$, where

$$\theta_n = \arctan(\tilde{k}/q_n). \quad (\text{B2})$$

It is easy to verify that in the energy window (B1)

$$\left| \frac{1 - z_{n,k} z_{n,\tilde{k}}}{z_{n,k} - z_{n,\tilde{k}}} \right| = 1. \quad (\text{B3})$$

We can now rewrite Eq. (A18) as

$$\tan(\tilde{k}L) = \frac{\sin \theta_n (1 - z_{n,k}^2)}{2z_{n,k} - (1 + z_{n,k}^2) \cos \theta_n} \quad (\text{B4})$$

and further simplify this expression by using that

$$\sin \theta_n = \frac{\tilde{k}/q_n}{\sqrt{1 + (\tilde{k}/q_n)^2}}, \quad (\text{B5})$$

$$\cos \theta_n = \frac{1}{\sqrt{1 + (\tilde{k}/q_n)^2}}. \quad (\text{B6})$$

After some algebra, we obtain

$$\tan(\tilde{k}L) = \frac{-i\tilde{k}k}{(\varepsilon - eV_{\text{barrier}})(\varepsilon - eV_{\text{gate}})/(\hbar v)^2 - q_n^2}. \quad (\text{B7})$$

The latter equation in combination with Eq. (A13) yields Eq. (7). Numerical solutions to Eq. (B7) are shown in Fig. 2.

By applying different voltages to the gate and the barriers we shift the energy bands of the graphene ribbon under the barriers with respect to that of the quantum dot. A bound state in the quantum dot is allowed once the energy of the state hits the band gap of the barriers. If the difference of the barrier and gate voltages $\Delta V = |V_{\text{barrier}} - V_{\text{gate}}|$ is less than the energy of the gap $2\hbar v|q_n|$ for n -th subband, \tilde{k} of a bound state lies in the interval $[-\tilde{k}_{\text{max}}, \tilde{k}_{\text{max}}]$, where \tilde{k}_{max} is found from the condition $\varepsilon(\tilde{k}_{\text{max}}) = V_{\text{barrier}} + \hbar v|q_n|$ and, therefore, $\tilde{k}_{\text{max}} = e\Delta V \sqrt{1 + 2\hbar v|q_n|/e\Delta V}$. The number of bound states (for a given subband index n) is proportional to the length of the quantum dot L and is given by $N = \lceil \tilde{k}_{\text{max}}L/\pi \rceil$ ($\lceil x \rceil$ is the integer just larger than x). The number of the bound states of the n -th subband is maximal, when the barrier-gate voltage difference equals the energy band gap ($\Delta V = 2\hbar v|q_n|$), and so $N_{\text{max}} = \lceil \sqrt{8}|q_n|L/\pi \rceil$. In the case of $\Delta V > 2\hbar v|q_n|$, the top of the valence band of the graphene ribbon under the barriers becomes higher than the bottom of the conduction band of the quantum dot, therefore, there are no bound states with energies $\varepsilon < eV_{\text{barrier}} - \hbar v|q_n|$ and $|\tilde{k}|$ of a bound state lies in the interval $[\tilde{k}_{\text{min}}, \tilde{k}_{\text{max}}]$, where \tilde{k}_{min} is found from the condition $\varepsilon(\tilde{k}_{\text{min}}) = V_{\text{barrier}} - \hbar v|q_n|$ ($\tilde{k}_{\text{min}} = e\Delta V \sqrt{1 - 2\hbar v|q_n|/e\Delta V}$), therefore, bound states lie in the energy window $eV_{\text{barrier}} - \hbar v|q_n| \leq \varepsilon \leq eV_{\text{barrier}} + \hbar v|q_n|$ (as shown in Fig. 2) and the number of the bound states is given by $N = \lceil \tilde{k}_{\text{max}}L/\pi \rceil - \lceil \tilde{k}_{\text{min}}L/\pi \rceil$.

With increasing the barrier-gate voltage difference, a m -th bound state appears at $\Delta V_0 = -\hbar v|q_n| + \hbar v \sqrt{q_n^2 + (\pi/L)^2(m-1)^2}$ with the energy $\varepsilon_m^{(0)} = V_{\text{gate}} + \Delta V_0 + \hbar v|q_n|$ and ends up at $\Delta V_1 = \hbar v|q_n| + \hbar v \sqrt{q_n^2 + (\pi/L)^2m^2}$ with the energy $\varepsilon_m^{(1)} = V_{\text{gate}} + \Delta V_1 - \hbar v|q_n|$ (see Fig. 2).

APPENDIX C: WAVE FUNCTION

Following Brey and Fertig [28], we write the wave function as

$$\Psi(x, y) = \begin{pmatrix} \Psi_A^{(K)}(x, y) \\ \Psi_B^{(K)}(x, y) \\ -\Psi_A^{(K')}(x, y) \\ -\Psi_B^{(K')}(x, y) \end{pmatrix} \quad (\text{C1})$$

and give solutions for each component separately. As mentioned above, the subscripts A and B refer to the two sublattices in the two-dimensional honeycomb lattice of carbon atoms and the superscripts K and K' refer to the two valleys in graphene. Note that the normalization condition [28]

$$\int dxdy [|\Psi_\mu^{(K)}(x, y)|^2 + |\Psi_\mu^{(K')}(x, y)|^2] = 1 \quad (\text{C2})$$

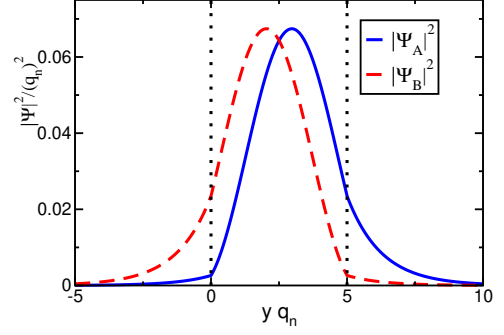


FIG. 7: **Ground-state wave function.** Normalized squared wave function $|\Psi_A|^2 = |\Psi_A^{(K)}|^2 = |\Psi_A^{(K')}|^2$ and $|\Psi_B|^2 = |\Psi_B^{(K)}|^2 = |\Psi_B^{(K')}|^2$ for the ground state solution of a dot of length $q_nL = 5$ with corresponding energy $\varepsilon = 1.101 \hbar v q_n$. Here, $e(V_{\text{barrier}} - V_{\text{gate}}) = 0.5 \hbar v q_n$. The dotted lines indicate the dot region $0 \leq y q_n \leq 5$.

(for $\mu = A, B$ each) finally determines the normalization constant of the wave function. With the ansatz (A12) we explicitly obtain the following components of the wave function

$$\Psi_A^{(K)}(x, y) = \begin{cases} \alpha_n z_{n,k} e^{iq_n x} e^{-iky}, \\ \beta_n e^{iq_n x} e^{iky} + \gamma_n z_{n,\tilde{k}} e^{iq_n x} e^{-iky}, \\ \delta_n e^{iq_n x} e^{ik(y-L)}, \end{cases} \quad (\text{C3})$$

$$\Psi_B^{(K)}(x, y) = \begin{cases} \alpha_n e^{iq_n x} e^{-iky}, \\ \beta_n z_{n,\tilde{k}} e^{iq_n x} e^{iky} + \gamma_n e^{iq_n x} e^{-iky}, \\ \delta_n z_{n,k} e^{iq_n x} e^{ik(y-L)}, \end{cases} \quad (\text{C4})$$

$$-\Psi_A^{(K')}(x, y) = \begin{cases} \alpha_n z_{n,k} e^{-iq_n x} e^{-iky}, \\ \beta_n e^{-iq_n x} e^{iky} + \gamma_n z_{n,\tilde{k}} e^{-iq_n x} e^{-iky}, \\ \delta_n e^{-iq_n x} e^{ik(y-L)}, \end{cases} \quad (\text{C5})$$

$$-\Psi_B^{(K')}(x, y) = \begin{cases} \alpha_n e^{-iq_n x} e^{-iky}, \\ \beta_n z_{n,\tilde{k}} e^{-iq_n x} e^{iky} + \gamma_n e^{-iq_n x} e^{-iky}, \\ \delta_n z_{n,k} e^{-iq_n x} e^{ik(y-L)}. \end{cases} \quad (\text{C6})$$

In the latter equations, the first line corresponds to the region in space, where $y < 0$, the second line to $0 \leq y \leq L$, and the third line to $y > L$. Thus, we obtain that

$$|\Psi_A^{(K)}(x, y)|^2 = |\Psi_A^{(K')}(x, y)|^2, \quad (\text{C7})$$

$$|\Psi_B^{(K)}(x, y)|^2 = |\Psi_B^{(K')}(x, y)|^2. \quad (\text{C8})$$

We now plot the normalized squared wave function of a ground-state solution and a excited-state solution of a dot with length $q_nL = 5$ in Figs. 7 and 8, respectively. These are obtained from Fig. 2 under the choice that $e(V_{\text{barrier}} - V_{\text{gate}}) = 0.5 \hbar v q_n$. Evidently, the ground-state solution has no nodes in the dot region, whereas the excited-state solution has nodes.

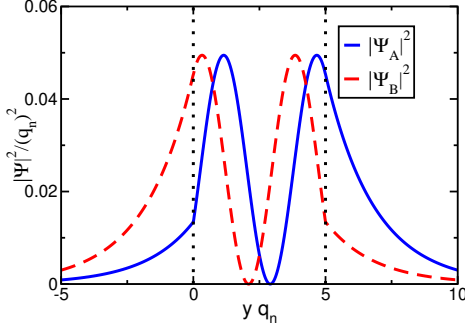


FIG. 8: **Excited-state wave function.** Normalized squared wave function $|\Psi_A|^2 = |\Psi_A^{(K)}|^2 = |\Psi_A^{(K')}|^2$ and $|\Psi_B|^2 = |\Psi_B^{(K)}|^2 = |\Psi_B^{(K')}|^2$ for the first excited state solution of a dot of length $q_n L = 5$ with corresponding energy $\varepsilon = 1.34 \hbar v q_n$. Here, $e(V_{\text{barrier}} - V_{\text{gate}}) = 0.5 \hbar v q_n$. The dotted lines indicate the dot region $0 \leq y q_n \leq 5$.

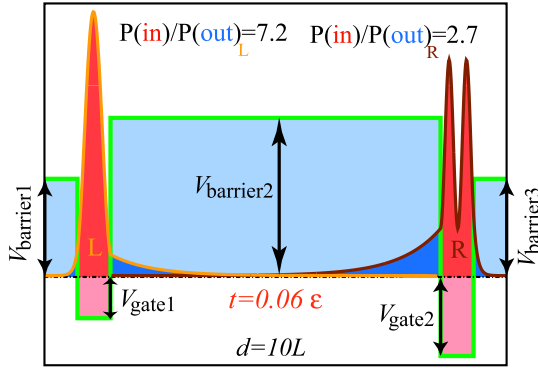


FIG. 9: **Long-distance coupling of a ground state and an excited state.** The normalized squared wave functions $|\Psi|^2 = |\Psi_A^{(K)}|^2 + |\Psi_A^{(K')}|^2 + |\Psi_B^{(K)}|^2 + |\Psi_B^{(K')}|^2$ of two qubits separated by a distance $d = 10L$, where L is the length of each quantum dot, are plotted next to each other. A ground state (of the series with the transverse quantum number $n = 0$) in the left dot is coupled to an excited state (of the same series with $n = 0$) in the right dot. The coupling is as large as $t = 0.06\varepsilon$, where ε is the ground-state energy of the left dot. Furthermore, the qubits are still highly localized, which can be seen from the ratio $P(\text{in})/P(\text{out})$. Here, $P(\text{in})$ is the probability of the electron to be inside the corresponding dot and $P(\text{out})$ is probability to be outside the dot in the barrier regions. The parameters chosen for the potential (in units of $\hbar v q_0/e$) are $V_{\text{barrier}1} = V_{\text{barrier}3} = 1$, $V_{\text{barrier}2} = 1.65$, $V_{\text{gate}1} = -0.5$, and $V_{\text{gate}2} = -0.9$.

APPENDIX D: LONG-DISTANCE COUPLING

1. Long-distance coupling of two qubits

Here, we discuss a particular example of long-distance coupling of two qubits separated by a distance d . The coupling

is achieved via a continuum of states in the valence band of the barrier region as shown in Fig.3(b) of the Letter. Therefore, the long-range coupling is enabled by the Klein paradox. In the weak tunneling regime, the hopping matrix element is given by

$$t \approx \varepsilon \int \Psi_L^\dagger(x, y) \Psi_R(x, y) dx dy, \quad (\text{D1})$$

where $\Psi_{L,R}(x, y) = \Psi(x, y \pm (d + L)/2)$ are the spinor wave functions of the left and right dots and ε is the single-particle energy of the coupled levels. The integration in transverse x -direction is trivial and just gives a factor W . The integration in longitudinal y -direction can be restricted to the integration window $y \in [-d/2, d/2]$ if the wave functions are predominantly localized in the dot regions. Then, the hopping matrix element can be estimated for $d \gtrsim L$ as

$$t \approx 4\varepsilon\alpha_0\delta_0^* W d z_{0,k} \exp(-d|k|), \quad (\text{D2})$$

where α_0 and δ_0 are wave function amplitudes specified in Eqs. (C3) – (C6). In Eq. (D2), we assumed that only levels of the series corresponding to the $n = 0$ transverse mode are coupled. It is easy to relax this assumption because, if higher transverse modes form bound states, then only modes with $n_L = n_R$ contribute to t , where $n_{L/R}$ is the transverse quantum number in the left/right dot. In Fig. 9, we demonstrate that a rather large coupling of $t = 0.06\varepsilon$ can be achieved over a distance as large as ten times the size of the quantum dots (see also Fig. 5 for comparison). Note that the qubits in this example are well localized in the corresponding dot regions: The probability of the electron in the left dot to be in the dot region $P(\text{in})$ is 7.2 times larger than to be in the barrier regions $P(\text{out})$. For the right dot, the ratio of $P(\text{in})/P(\text{out}) = 2.7$ is a bit smaller but the electron is still predominantly localized in the dot region.

2. Long-distance coupling in multiple quantum dot setup

In Fig.6, we propose a triple quantum dot setup in which dot 1 and dot 3 are strongly coupled and the center dot 2 is decoupled by detuning. It is important that dot 1 and dot 3 are coupled via the valence band states of dot 2 and not via the (detuned) qubit level of dot 2. Otherwise, the spin of the decoupled qubit level would be affected by the coupling of the other qubits which is unwanted in the proposed long-distance coupling scheme. We assume that the gates that put the three dots in the Coulomb blockade regime are set in such a way that cotunneling processes from dot 1 via dot 2 to dot 3 happen in the following order: First, an electron tunnels from dot 2 to dot 3 and then an electron tunnels from dot 1 to dot 2. The system is described by the Hamiltonian

$$H = H_0 + H_T, \quad (\text{D3})$$

where the kinetic term describes three qubit levels ($\alpha = 1, 2, 3$) and the continuum of states in the valence band of dot 2

$$H_0 = \sum_{\alpha=1-3} \sum_{\sigma=\uparrow,\downarrow} E_{\alpha,\sigma} a_{\alpha,\sigma}^\dagger a_{\alpha,\sigma} + \sum_k \sum_{\sigma=\uparrow,\downarrow} \varepsilon_{k,\sigma} b_{k,\sigma}^\dagger b_{k,\sigma} \quad (\text{D4})$$

and the tunnelling Hamiltonian reads

$$H_T = t \sum_{\sigma} (a_{1,\sigma}^{\dagger} a_{2,\sigma} + a_{2,\sigma}^{\dagger} a_{3,\sigma} + \text{H.c.}) + t \sum_{k,\sigma} (a_{1,\sigma}^{\dagger} b_{k,\sigma} + b_{k,\sigma}^{\dagger} a_{3,\sigma} + \text{H.c.}). \quad (\text{D5})$$

In Eq. (D4), $a_{\alpha,\sigma}$ and $b_{k,\sigma}$ annihilate electrons with spin σ in the qubit level of dot α and in the valence band of dot 2, respectively. We assume that $E_{1,\sigma} = E_{3,\sigma}$ (i.e. qubit 1 and qubit 3 are on resonance) and $\Delta\epsilon_1 = E_{2,\sigma} - E_{1,\sigma} \approx E_{\text{gap}} = 2\hbar v q_0$ (see Fig. 6). In Eq. (D5), we make the approximation that all tunnelling matrix elements t depend only very weakly on energy and are real. The transmission rate from an initial state $|i\rangle$ to a final state $|f\rangle$ can be calculated using Fermi's golden rule

$$W_{fi} = \frac{2\pi}{\hbar} |\langle f | T(\epsilon_i) | i \rangle|^2 \delta(\epsilon_f - \epsilon_i) \quad (\text{D6})$$

with the transition matrix given by (up to second order in H_T)

$$T(\epsilon) = H_T + H_T \frac{1}{\epsilon + i\eta - H_0} H_T + \dots \quad (\text{D7})$$

We can put $\eta = 0$ in the latter equation because we are only interested in off-resonant cotunnelling processes. This means that $\Delta\epsilon_2$ (see Fig. 6) should be finite because we want to have well-localized qubit states. The corresponding matrix elements of the T-matrix (D7) may be written as

$$(T(\epsilon))_{k,k'} = (H_T)_{k,k'} + \sum_{k''} (H_T)_{k,k''} \frac{1}{\epsilon - \epsilon_{k''}} (H_T)_{k'',k'} + \dots \quad (\text{D8})$$

Now, we want to calculate $|T_{13}|^2 \equiv |\langle 3 | T(E_{1,\sigma}) | 1 \rangle|^2$, where $|1\rangle$ and $|3\rangle$ are the ground states of qubit 1 and 3, respectively. The lowest non-vanishing contribution of $|T_{13}|^2$ is of cotunnelling type, i.e., of fourth order in t . It is possible to separate the different contributions to $|T_{13}|^2$ into three terms, namely

$$|T_{13}|^2 = |T_{13}^{(QB)}|^2 + |T_{13}^{(VB)}|^2 + 2 \text{Re} [(T_{13}^{(QB)})^* T_{13}^{(VB)}]. \quad (\text{D9})$$

In the latter equation, $|T_{13}^{(QB)}|^2$ determines the transition rate via the qubit level of dot 2 (the unwanted process), $|T_{13}^{(VB)}|^2$ determines the transition rate via the continuum of states in the valence band of dot 2 (the wanted process), and $2 \text{Re} [(T_{13}^{(QB)})^* T_{13}^{(VB)}]$ is the interference term of the two paths. It is straightforward to derive that (for a given spin σ of qubit 2)

$$T_{13}^{(QB)}(E_{1,\sigma}) = \frac{t^2}{E_{1,\sigma} - E_{2,\sigma}}. \quad (\text{D10})$$

This has to be compared with

$$T_{13}^{(VB)}(E_{1,\sigma}) = t^2 \int_{E_{\text{gap}}/2}^{\Delta} dE \frac{\nu_0(E)}{E_{1,\sigma} - E} \approx -\frac{Lt^2}{\pi\hbar v} \ln(4\Delta/E_{\text{gap}}), \quad (\text{D11})$$

where

$$\nu_0(E) = \frac{L}{\hbar v \pi} \frac{E}{\sqrt{E^2 - (E_{\text{gap}}/2)^2}} \quad (\text{D12})$$

is the density of states of the mode $n = 0$ with $E_{\text{gap}} = 2\hbar v q_0$. In Eq. (D11), we integrate over the whole band width of the valence band (bounded by $\Delta \approx 6 \text{ eV}$). The approximate result in the second line of Eq. (D11) holds for the hierarchy of energies $\Delta \gg E_{\text{gap}} \gg E_{1,\sigma}$. (In a more general case, the integral in Eq. (D11) can still be evaluated analytically but yields a less compact expression.)

The contribution coming from $|T_{13}^{(QB)}|^2$ is evidently the smallest term of the three terms on the rhs of Eq. (D9). If we want to compare the rate that does not affect the spin of the qubit level in dot 2 (which we call Γ_{VB}) with the largest of the rates that does affect the spin of the qubit level in dot 2 (which we call Γ_{QB}), we can estimate

$$\frac{\Gamma_{\text{VB}}}{\Gamma_{\text{QB}}} = \frac{|T_{13}^{(VB)}|^2}{|2 \text{Re} [(T_{13}^{(QB)})^* T_{13}^{(VB)}]|} \approx \frac{L}{W} \ln(4\Delta/E_{\text{gap}}). \quad (\text{D13})$$

The latter result is Eq. (9). It shows that by increasing the aspect ratio L/W we can increase the weight of the coupling via the valence band states of dot 2 (which is wanted) as compared to the weight of the coupling via the qubit state of dot 2 (which is unwanted).

APPENDIX E: DECOHERENCE

Finally, we give some arguments and rough estimates for the spin decoherence in graphene. It is generally believed that spin-orbit effects are weaker in carbon than in GaAs due to the lower atomic weight. Therefore, the dominating mechanism for decoherence will be the hyperfine coupling to the nuclear spins that are present in the material.

The coherence time given by the hyperfine coupling can be estimated as [12] $t \approx \sqrt{N}/cA^{-1}$, where N is the number of atoms in the dot (for a typical graphene dot, $N \approx 10^4$), cN is the number of atoms per dot with a nuclear spin, and A the coupling constant of the hyperfine interaction. Since we mainly deal with π orbitals in graphene, the contact hyperfine interaction is strongly reduced and the hyperfine interaction is dominated by its dipolar part. From the best available calculations for the dipolar hyperfine matrix elements [32, 33], one obtains

$$A_{\text{dip}} = \frac{8}{5} \frac{\mu_0}{4\pi} \mu_B \mu \left\langle \frac{1}{r^3} \right\rangle \approx 0.38 \mu\text{eV}, \quad (\text{E1})$$

where μ is the nuclear magneton of ^{13}C , μ_B is the Bohr magneton, and μ_0 the vacuum dielectric constant. This estimated value for A_{dip} is smaller than $A_{\text{GaAs}} \approx 90 \mu\text{eV}$ by more than two orders of magnitude. The natural abundance of ^{13}C is about $c \approx 1\%$ which yields, with the values quoted above, a coherence time of approximately $t \approx 10 \mu\text{s}$, about a thousand times longer than in GaAs. Unlike in GaAs, this value can be

improved by isotopic purification. Reducing the ^{13}C content by a factor of about 100 already decreases the average number of nuclear spins per dot to about one. This allows for a

preselection of the dots without any nuclear spin to be used as qubits.

-
- [1] Loss, D. & DiVincenzo, D.P. Quantum computation with quantum dots. *Phys. Rev. A* **57**, 120-126 (1998).
 - [2] Elzerman, J.M. *et al.* Single-shot read-out of an individual electron spin in a quantum dot. *Nature* **430**, 431-435 (2004).
 - [3] Hanson, R. *et al.* Single-shot readout of electron spin states in a quantum dot using spin-dependent tunnel rates. *Phys. Rev. Lett.* **94**, 196802 (2005).
 - [4] Petta, J.R. *et al.* Coherent manipulation of coupled electron spins in semiconductor quantum dots. *Science* **309**, 2180-2184 (2005).
 - [5] Koppens, F.H.L. *et al.* Driven coherent oscillations of a single electron spin in a quantum dot. *Nature* **442**, 766-771 (2006).
 - [6] Khaetskii, A.V. & Nazarov, Y.V. Spin relaxation in semiconductor quantum dots. *Phys. Rev. B* **61**, 12639-12642 (2000).
 - [7] Khaetskii, A.V. & Nazarov, Y.V. Spin-flip transitions between Zeeman sublevels in semiconductor quantum dots. *Phys. Rev. B* **64**, 125316 (2001).
 - [8] Golovach, V.N., Khaetskii, A.V. & Loss, D. Phonon-induced decay of the electron spin in quantum dots. *Phys. Rev. Lett.* **93**, 016601 (2004).
 - [9] Burkard, G., Loss, D. & DiVincenzo, D.P. Coupled quantum dots as quantum gates. *Phys. Rev. B* **59**, 2070-2078 (1999).
 - [10] Erlingsson, S.I., Nazarov, Y.V. & Fal'ko V.I. Nucleus-mediated spin-flip transitions in GaAs quantum dots. *Phys. Rev. B* **64**, 195306 (2001).
 - [11] Khaetskii, A.V., Loss, D. & Glazman, L. Electron spin decoherence in quantum dots due to interaction with nuclei. *Phys. Rev. Lett.* **88**, 186802 (2002).
 - [12] Coish, W.A. & Loss, D. Hyperfine interaction in a quantum dot: Non-Markovian electron spin dynamics. *Phys. Rev. B* **70**, 195340 (2004).
 - [13] Johnson, A.C. *et al.* Triplet-singlet spin relaxation via nuclei in a double quantum dot. *Nature* **435**, 925-928 (2005).
 - [14] Koppens, F.H.L. *et al.* Control and detection of singlet-triplet mixing in a random nuclear field. *Science* **309**, 1346-1350 (2005).
 - [15] Min, H. *et al.* Intrinsic and Rashba spin-orbit interactions in graphene sheets. *Phys. Rev. B* **74**, 165310 (2006).
 - [16] Novoselov, K.S. *et al.* Electric field effect in atomically thin carbon films. *Science* **306**, 666-669 (2004).
 - [17] Novoselov, K.S. *et al.* Two-dimensional gas of massless Dirac fermions in graphene. *Nature* **438**, 197-200 (2005).
 - [18] Zhang, Y., Tan, Y.-W., Stormer, H.L. & Kim, P. Experimental observation of the quantum Hall effect and Berry's phase in graphene. *Nature* **438**, 201-204 (2005).
 - [19] Cheianov, V.V. & Fal'ko, V.I. Selective transmission of Dirac electrons and ballistic magnetoresistance of $n-p$ junctions in graphene. *Phys. Rev. B* **74**, 041403(R) (2006).
 - [20] Dombay, N. & Calogeracos, A. Seventy years of the Klein paradox. *Phys. Rep.* **315**, 41-58 (1999).
 - [21] Katsnelson, M.I., Novoselov, K.S. & Geim, A.K. Klein paradox in graphene. *Nature Phys.* **2**, 620-625 (2006).
 - [22] McClure, J.W. Diamagnetism of graphite. *Phys. Rev.* **104**, 666-671 (1956).
 - [23] Semenoff, G.W. Condensed-matter simulation of a three-dimensional anomaly. *Phys. Rev. Lett.* **53**, 2449-2452 (1984).
 - [24] DiVincenzo, D.P. & Mele, E.J. Self-consistent effective-mass theory for intralayer screening in graphite intercalation compounds. *Phys. Rev. B* **29**, 1685-1694 (1984).
 - [25] Silvestrov, P.G. & Efetov, K.B. Quantum dots in graphene. *Phys. Rev. Lett.* **98**, 016802 (2007).
 - [26] Nilsson, J., Castro Neto, A.H., Guinea, F. & Peres, N.M.R. Transmission through a biased graphene bilayer barrier. Preprint at www.arXiv.org/cond-mat/0607343 (2006).
 - [27] De Martino, A., Dell'Anna, L. & Egger, R. Magnetic confinement of massless Dirac fermions in graphene. Preprint at www.arXiv.org/cond-mat/0610290 (2006).
 - [28] Brey, L. & Fertig, H.A. Electronic states of graphene nanoribbons studied with the Dirac equation. *Phys. Rev. B* **73**, 235411 (2006).
 - [29] Tworzydło, J., Trauzettel, B., Titov, M., Rycerz, A. & Beenakker, C.W.J. Quantum-limited shot noise in graphene. *Phys. Rev. Lett.* **96**, 246802 (2006).
 - [30] Grabert, H. & Devoret, M.H. (eds.) *Single Charge Tunnelling*. (Plenum, New York, 1991).
 - [31] Svore, K. M., Terhal, B. M. & DiVincenzo, D. P. Local fault-tolerant quantum computation. *Phys. Rev. A* **72**, 022317 (2005).
 - [32] Tang, X.-P. *et al.*, Electronic structures of single-walled carbon nanotubes determined by NMR. *Science* **288**, 492-494 (2000).
 - [33] Antropov, V. P., Mazin, I. I., Andersen, O. K., Liechtenstein, A. I. & Jepsen, O., Dominance of the spin-dipolar NMR relaxation mechanism in fullerene superconductors. *Phys. Rev. B* **47**, 12373-12376 (1993).

Acknowledgements We thank H.A. Fertig and L.M.K. Vandersypen for discussions and acknowledge support from the Swiss NSF, NCCR Nanoscience, DARPA, ONR, and JST ICORP.